

Original Research

Metabolic Landscape of Osteosarcoma: Reprogramming of Lactic Acid Metabolism and Metabolic Communication

Linbang Wang^{1,2,3,†}, Xinyu Dou^{1,2,3,†}, Linzhen Xie⁴, Xuchang Zhou⁵, Yu Liu^{1,2,3},
Jingkun Liu^{6,*}, Xiaoguang Liu^{1,2,3,*}¹Department of Orthopedics, Peking University Third Hospital, 100191 Beijing, China²Beijing Key Laboratory of Spinal Disease Research, 100191 Beijing, China³Engineering Research Center of Bone and Joint Precision Medicine, Ministry of Education, 100191 Beijing, China⁴Peking University Fourth School of Clinical Medicine, 100035 Beijing, China⁵School of Sport Medicine and Rehabilitation, Beijing Sport University, 100084 Beijing, China⁶Department of Orthopedics, Honghui Hospital, Xi'an Jiaotong University, 710054 Xi'an, Shaanxi, China*Correspondence: heluxue68@hotmail.com (Jingkun Liu); xglius@163.com (Xiaoguang Liu)

†These authors contributed equally.

Academic Editor: Marco Falasca

Submitted: 9 August 2023 Revised: 30 September 2023 Accepted: 12 October 2023 Published: 22 February 2024

Abstract

Background: Lactic acid, previously regarded only as an endpoint of glycolysis, has emerged as a major regulator of tumor invasion, growth, and the tumor microenvironment. In this study, we aimed to explore the reprogramming of lactic acid metabolism relevant to osteosarcoma (OS) microenvironment by decoding the underlying lactic acid metabolic landscape of OS cells and intercellular signaling alterations. **Methods:** The landscape of OS metabolism was evaluated using single-cell gene expression data, lactic acid metabolism clustering, and screening of the hub genes in lactic acid metabolism of OS samples using transcriptome data. The role of the hub gene NADH:Ubiquinone Oxidoreductase Complex Assembly Factor 6 (*NDUFAF6*) was validated with *in vitro* studies and patient experiments. **Results:** Single-cell RNA sequencing data validated a lactic acid metabolism-high subcluster in OS. Further investigation of intercellular communications revealed a unique metabolic communication pattern between the lactic acid metabolism-high subcluster and other subclusters. Next, two lactic acid metabolic reprogramming phenotypes were defined, and six lactic acid metabolism-related genes (LRGs), including the biomarker *NDUFAF6*, were screened in OS. *In vitro* studies and patient experiments confirmed that *NDUFAF6* is a crucial lactic acid metabolism-associated gene in OS. **Conclusions:** The patterns of lactic acid metabolism in OS suggested metabolic reprogramming phenotypes relevant to the tumor microenvironment (TME) and identified *NDUFAF6* as an LRG prognostic biomarker.

Keywords: metabolic reprogramming; osteosarcoma; lactic acid metabolism; metabolic communication; *NDUFAF6*

1. Introduction

Osteosarcoma (OS) is one of the most common malignant bone tumor worldwide [1]. Notably, OS is characterized by the presence of transformed osteoblasts that produce poorly differentiated bones and osteoids. The pathology of OS has a high degree of heterogeneity, and different histological types of OS exhibit distinct biological and molecular characteristics [2]. The pathogenesis of OS has not been clearly clarified; however, multiple genetic and environmental risk factors, such as age, radiation, and gene mutations, have been found to be associated with osteosarcomagenesis and tumor progression [3]. OS exhibits a high propensity for local invasion and distant metastasis (most commonly in the lungs), as well as recurrence. The 5-year survival rate of OS has reached 70% in the nonmetastatic stage since the introduction of chemotherapy [4]. However, the overall survival rate among patients with metastasis remains at approximately 20% and has not improved over the past forty years [5,6]. Therefore, a better understanding of the molecular mechanisms uncovering OS progression is critical for the development of customized treatment strategies.

Metabolic reprogramming of tumor cells in response to stress facilitates tumor progression, and the inhibition of metabolic reprogramming of tumor cells has been shown to reduce cell proliferation and invasion [7]. Tumor metabolic reprogramming dynamically changes during cancer progression, participates in the reprogramming of the tumor microenvironment, and leads to the metabolic reprogramming of immune cells in the microenvironment [8]. For example, the glycolytic conversion (Warburg effect) of tumor cells to the regulatory adaptation of lactic acid metabolism contributes to the epithelial–mesenchymal transformation of tumor cells and activation of T cells. It is also regulated by multiple factors in the microenvironment, including cytokines [9–11]. Therefore, it is necessary to map tumor metabolic reprogramming from the perspective of tumor microenvironment.

Tumors exhibit high metabolic heterogeneity [12]. However, the interaction between metabolic phenotypes and the tumor microenvironment is not comprehensively understood. Notably, it has not yet been determined whether the heterogeneity of tumor metabolism can be used



to classify OS. Single-cell transcriptomics provides a platform for exploring the cellular heterogeneity of metabolism and characteristics of the microenvironment. The construction of intercellular communication features enables systematic elucidation of the regulatory mechanisms of metabolic reprogramming in the tumor microenvironment. In this study, the landscape of lactic acid metabolic communication in OS was revealed and hub genes involved in this biological process were screened.

2. Materials and Methods

2.1 Data Set Acquisition

To research the single-cell level metabolism features of and their communications patterns, the single cell RNA (scRNA) sequencing datasets from the Gene Expression Omnibus database (<https://www.ncbi.nlm.nih.gov/geo/query/acc.cgi?acc=GSE152048>) were integrated. OS transcriptome sequencing data with updated clinical data were downloaded from The Cancer Genome Atlas (TARGETs) (<https://ocg.cancer.gov/programs/target>) and the GEO database (<https://www.ncbi.nlm.nih.gov/gds/?term=GSE16088>).

2.2 Single-Cell Transcriptome Standard Analysis

The scran R package (version 4.3) was utilized for normalization, and standard log-normalization was conducted on multiple scRNA datasets to identify variable features in each individual [13,14]. Anchors between datasets were determined using the FindIntegrationAnchors (Seurat v5) function and returned as Seurat objects for downstream analysis. The subtypes of OS and immune cells were individually identified using SingleR (version 3.1.7) [15]. The Monocle2 (version 2.4.0) algorithm was used to construct a single-cell pseudo-time trajectory and identify the expression of genes that changed as the cells underwent differentiation. The interaction between different OS subclusters was investigated using NicheNet (version 1.0) [16], which utilizes an incident ligand-based method to identify ligand activity in receiving cells.

2.3 Consensus Clustering for Lactate Metabolism Gene (LAMG) Subtypes

We performed a consensus clustering algorithm for the unsupervised classification of OS samples using the ConsensusClusterPlus R package (v1.50.0) based on LAMGs [17]. K-means (km) cluster method was performed with repeated iterations of 1000 to ensure dependability, and the Gene Set Variation Analysis (GSVA) package (v1.34.0) [18] was used to illustrate the differential biological functions among the two clusters. Single-sample gene set enrichment analysis (ssGSEA) was used to elucidate the infiltration of immune cells and different subclusters of OS in each sample.

2.4 Screening and Validation of Diagnostic LAMGs

Multiple machine learning algorithms, including the random forest (RF) and support vector machine (SVM)-

recursive feature elimination (RFE), were used to construct prediction signatures and screen candidate diagnostic genes. The “randomForest” R package (version 4.7-1.1) were used to further screen genes, the RF screens gene features based on Gini coefficient [19]. SVM-RFE is a support vector machine that uses a backward sequential selection algorithm. It ranks each feature by its score and removes the feature with the lowest score until the required number of features are screened. Weighted gene co-expression network analysis (WGCNA) was subsequently performed on the OS cohort A data using the corresponding R package to identify the modules associated with interesting features [20], and a topological overlap matrix (TOM) was first obtained using the adjacency matrix. Next, genes were split into various gene modules, outliers were removed by clustering analysis, and the optimal value of the soft threshold β was used to construct a scale-free network. Gene significance (GS) and module membership (MM) were calculated and used for gene screening. The intersecting gene among the three screened gene sets was considered a candidate diagnostic gene.

2.5 Cell Culture

The 143B human OS cell line were required and were cultured as previously described [21]. The 143 cell line was validated by STR profiling and tested negative for mycoplasma. Cells were all cultured in a humidified incubator at 37 °C and 5% CO₂. Lactic acid (100 µg/mL, Product Number : L122090, Brand : aladdin, CAS-No.: 79-33-4, Shanghai Aladdin Biochemical Technology Co., Ltd. No. 809) was added to the medium to stimulate the OS cells. To inhibit the expression of *NDUFAF6*, OS cells were transfected with *NDUFAF6* siRNA for 24 h using the INVI DNA RNA transfection reagent (Retinotech, CAS-No: IV1216025, Shanghai Nonin Biological Technology Co., Ltd.). The siRNA sequences used were as follows: si-*NDUFAF6*-specific siRNA: 5'-AGUUUUUUUCCAAAACUGCAU-3' and 'Non-sense' (Control): 5'-UUCUCCGAACGUGUCACGUTT-3'.

2.6 Cell Viability Assay

143B cells (1×10^4) were seeded in 96-well plates and cultured for 48 h. Next, the medium was removed and 10 µL Cell Counting Kit-8 (CCK-8) solution (Cat. No B34302, Selleck, Houston, TX, USA) was added to the wells according to the manufacturer's protocol (Beyotime, China), and the absorbance at 450 nm was measured after incubation for 4 h at 37 °C.

2.7 Transwell Experiment

The Transwell system was applied for the cell invasion experiment. 143B cells were seeded into the upper chamber with extracellular matrix (Cat. No: 354243, BD Biosciences, San Jose, CA, USA) coated. The cells trapped the filter were fixed and stained with crystal violet solution after incubation. The cells were photographed using

a phase-contrast microscope (Cat. No: CX43, Olympus, Tokyo, Japan), and the cell numbers were counted.

2.8 Assessment of Cells Metabolic Status

Seahorse XF24 Analyzer (Cat. No: XF24, Agilent Technologies, Santa Clara, CA, USA) were used to assess the metabolic status of the cells. To measure the extracellular acidification rate (ECAR), the Mito Stress Test kit (Cat. No: 103010-100 Agilent Technologies, #103,015, Santa Clara, CA, USA) was applied after siRNA treatment. After enabling the cells to acclimate to the temperature and pH equilibration, the cells were loaded into the XF24 Analyzer and measurements from T = 0 to T = 100 min were recorded. The injection procedure was as follows: first, oligomycin (Cat. No: 103010-100 Agilent Technologies, #103,015, Santa Clara, CA, USA) at the concentration of 1 μ M; next, carbonyl cyanide m-chlorophenylhydrazone (Cat. No: 103010-100 Agilent Technologies, #103,015, Santa Clara, CA, USA) at the concentration of 1 μ M; then, rotenone (Cat. No: 103010-100 Agilent Technologies, #103,015, Santa Clara, CA, USA) and antimycin A (Cat. No: 103010-100 Agilent Technologies, #103,015, Santa Clara, CA, USA) at the concentration of 0.5 μ M.

2.9 Patients

OS tissues were all surgically resected from 12 patients at Honghui Hospital between January 2023 and March 2023. The inclusion criteria were as follow: a pathological diagnosis of OS and tumor resection, while the exclusion criteria were as follow: metastasis, recurrence, incomplete clinical data, or an unknown diagnosis. Adjacent tissues (n = 12) were collected from the same patients. Informed consent was obtained from all patients in this study. This study was approved by the Ethics Committee of Honghui Hospital (Approval Number: 202303051) and was conducted with the Declaration of Helsinki in accordance.

2.10 Quantitative Real Time Polymerase Chain Reaction (qRT-PCR)

Total RNA was isolated from 143B cells and human tissues by applying a UNIQ-10 column RNA Extraction Kit (Cat. No: B511321-0020, Sangon Biotech, China). Reverse transcription was performed by the RR047 cDNA Synthesis Kit (Cat. No: K1621, TaKaRa, China). The qRT-PCR was conducted on a 7500 Real-Time PCR System (Cat. No:4362143 Applied Biosystems, Foster City, CA, USA) using 2 \times Power SYBR[®] Green PCR Master Mix (Cat. No: 4309155, Invitrogen, USA). Gene expression levels were normalized to *GAPDH* expression levels. The following primer sequences were used: *TIMMDC1*-F (5'-GGAAGTCCTTGAGGAGCGTC-3'), *TIMMDC1*-R (5'-CATCAGCAGGCCTCTACAG-3'), *NDUFAF1*-F (5'-AGTGGCTTCTCCTGGCAAAG-3'), *NDUFAF1*-R (5'-TCCCCACGTACACGGAGATA-3'), *NDUFAF6*-F (5'-GAACTGGCTCAGGCTGGTTA-3'),

R (5'-GTGTGCTTGACTGGCAATGT-3'), *CARS2*-F (5'-TGCATTCTGGGCATTTGCAC-3'), *CARS2*-R (5'-ACACCATGCAAGGTAGCCTC-3'), *NDUFAF3*-F (5'-CTCGCGCTACGTAGCTTGTA-3'), *NDUFAF3*-R (5'-TCCTGGTGGAGGGATGAGAG-3'), *GAPDH*-F (5'-GAGAAGGCTGGGGCTCATT-3'), and *GAPDH*-R (5'-GTCAAAGGTGGAGGAGTGGG-3').

2.11 Immunohistochemistry Staining

Surgical specimens of tissues were cut to the thickness of 4 μ m and prepared on slides. Immunohistochemistry (IHC) were conducted to evaluate NDUFAF6 expression as follows: Dewaxing and endogenous horseradish peroxidase was inactivated, then the tissues were subjected to antigen repair. The tissue was then closed with Blocking Buffer contained phosphate-buffered solution. then a rabbit anti-NDUFAF6 antibody (ab150975, abcam, 152 Grove Street, Waltham, MA 02453, USA) was diluted and incubated. Finally, the tissues were washed and were murined with secondary antibody HRP (ab97051, abcam, 152 Grove Street, Waltham, MA 02453, USA).

3. Results

3.1 Metabolic Landscape of OS at Single-Cell Level

To reveal the diversity of cellular components in OS, analysis of OS scRNA-seq results was conducted. Single-cell transcriptome data were firstly clustered into 20 major clusters with the resolution of 0.5; combining with the chromosomal copy number variation (CNV) results that were calculated by inferCNV, malignant cells were identified [22] (Fig. 1A), and seven main segregated cell clusters, including cancer-associated fibroblasts (CAFs), dendritic cells, endothelial cells, malignant cells, tumor-associated macrophages (TAMs), T cells, and regulatory T cells (Tregs), were identified (Fig. 1B) using unbiased clustering of cells by using t-distributed stochastic neighbor embedding (t-SNE) analyses; the cell type of clusters were defined by singleR [15]. Next, we scanned the seven major metabolism processes that reportedly to play vital roles in the tumor progression, including lactate metabolism (Fig. 1C) [23], which refers to the metabolic process that osteosarcoma use lactate as their nutritional source and obtain energy through the tricarboxylic acid cycle, fatty acid metabolism (Fig. 1D) [24], retinoic acid metabolism (Fig. 1E) [25], cholesterol metabolism (Fig. 1F) [26], butyrate metabolism (Fig. 1G) [27], aspartate metabolism (Fig. 1H) [28], and glycolysis (Fig. 1I) [29], which refers to the metabolism process that produce lactic acid through glycolysis metabolism, by evaluating the overall expression levels of related gene sets in each cell. The expression levels of genes that related to lactate, fatty acid, glycerolipid, butyrate, and glycolysis metabolism were relatively high; however, the expression levels of cholesterol metabolism-related genes were relatively low. Subsequently, we focused on non-malignant stromal and immune cells in the OS microenvironment and found that the level of lactate

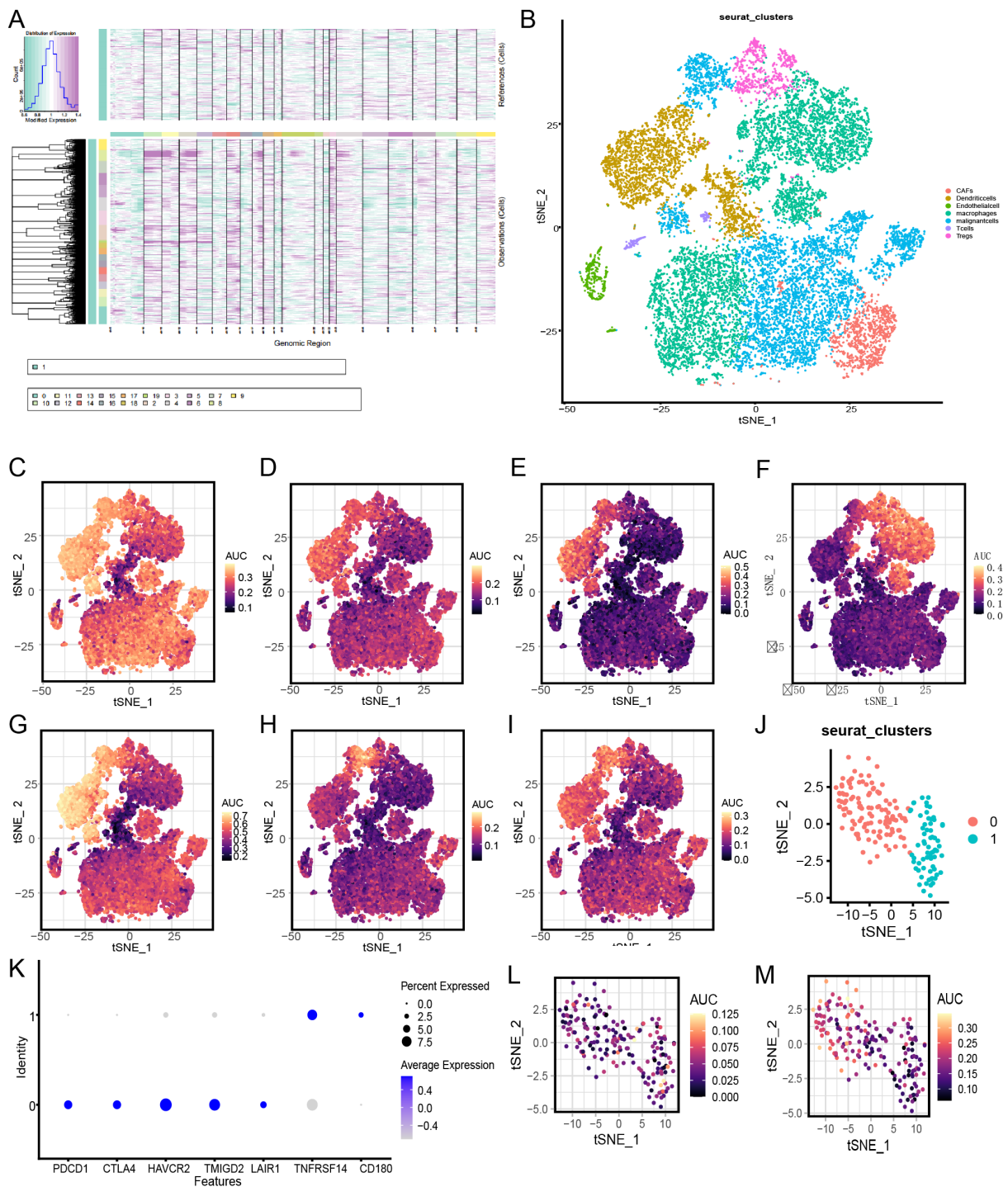


Fig. 1. Osteosarcoma tumor microenvironment (TME) and metabolism analysis. (A) The hierarchical heatmap shows copy number variation (CNV) from the osteosarcoma sample. (B) t-distributed stochastic neighbor embedding (t-SNE) plot shows the six cell clusters from the osteosarcoma sample. (C) t-SNE plot shows the lactate metabolism from the osteosarcoma sample. (D) t-SNE plot shows the fatty acid metabolism from the osteosarcoma sample. (E) t-SNE plot shows the retinoic acid metabolism from the osteosarcoma sample. (F) t-SNE plot shows the cholesterol metabolism from the osteosarcoma sample. (G) t-SNE plot shows the butyrate metabolism from the osteosarcoma sample. (H) t-SNE plot shows the aspartic metabolism from the osteosarcoma sample. (I) t-SNE plot shows the glycolysis metabolism from the osteosarcoma sample. (J) t-SNE plot shows the two T cell subclusters. (K) Dot plots showing the T cell signature gene expression across the two T cell subclusters. (L) t-SNE plot shows the lactic acid metabolism across the two T cell subclusters. (M) t-SNE plot shows the glycolysis metabolism across the two T cell subclusters. AUC, area under the curve; CAFs, cancer-associated fibroblasts.

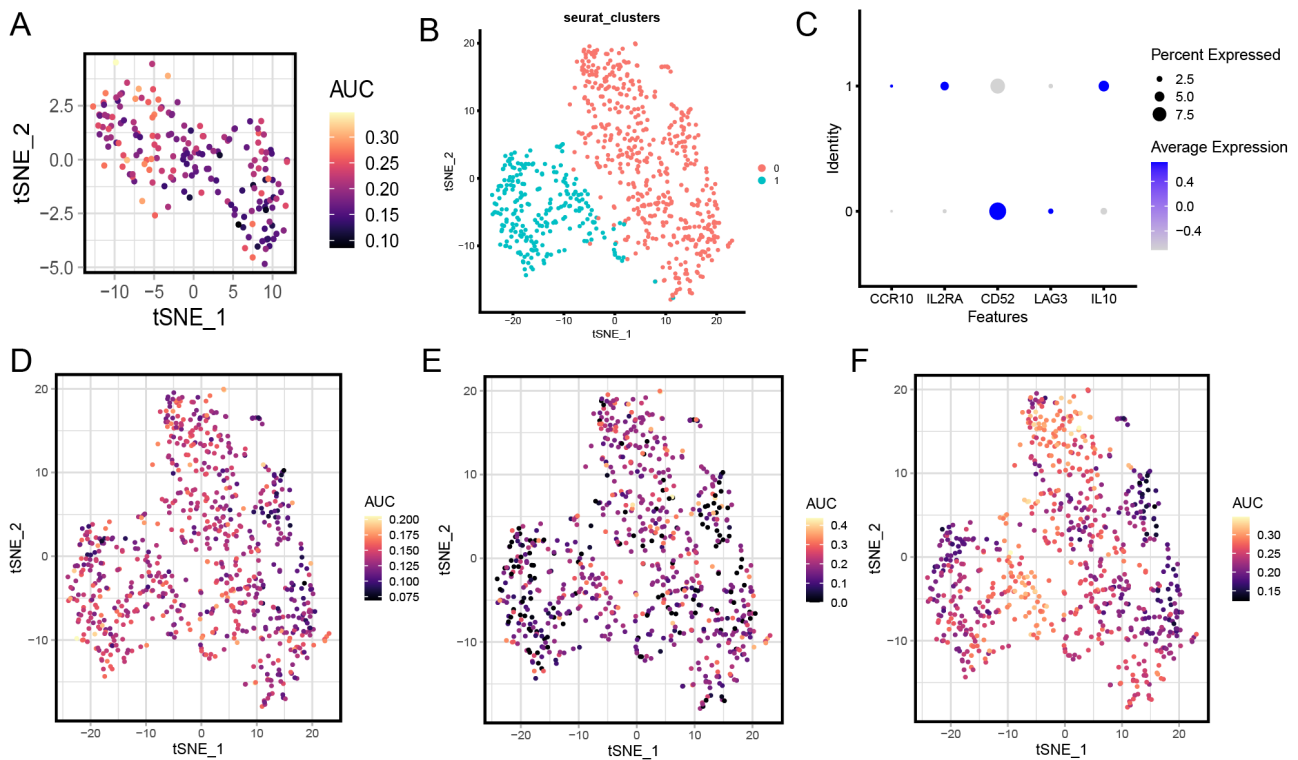


Fig. 2. Metabolism analysis of regulatory T cells (Tregs). (A) t-SNE plot shows the hypoxia metabolism across the two T cell subclusters. (B) t-SNE plot shows the two Treg cell subclusters. (C) Dot plots showing the Treg cell signature gene expression across the two T cell subclusters. (D) t-SNE plot shows the lactic acid metabolism across the two Treg cell subclusters. (E) t-SNE plot shows the glycolysis metabolism across the two Treg cell subclusters. (F) t-SNE plot shows the hypoxia metabolism across the two Treg cell subclusters.

metabolism was relatively low in T cells and dendritic cells, level of fatty acid metabolism was relatively high in dendritic cells, level of retinoic acid metabolism was relatively high in dendritic cells, level of cholesterol metabolism was relatively high in Tregs and TAMs, level of butyrate metabolism was relatively high in dendritic cells, level of aspartic acid metabolism was relatively high in Tregs, and level of glycolytic metabolism was relatively high in TAMs and Tregs.

Based on the previously reported key role of metabolism in the functional activation of T cells and Tregs [30,31], we further subdivided these two cell types. The results showed that T cells could be divided into two subclusters (Fig. 1J). As shown in Fig. 1K, cluster 0 T cells were defined as depletion T cells, according to the high expression levels of T cell depletion-related markers, including programmed cell death protein 1 (*PDCDI*), cytotoxic T-lymphocyte-associated protein 4 (*CTLA4*), and hepatitis A Virus Cellular Receptor 2 (*HAVCR2*) [32], and cluster 1 T cells were recognized as functional T cells based on the high expression level of TNF Receptor Superfamily Member 14 (*TNFRSF14*), which is known as a marker of antigen-presenting cell (APC) T cell activation [33]. Next, combined with previous description of the T cell metabolism features in TME [34], the key metabolic characteristics of

these two T cell subsets were observed, including lactic acid, glycolysis, and hypoxia metabolism [35]. The level of lactic acid metabolism was relatively low in depletion T cell and functional T cell clusters (Fig. 1L). The glycolysis metabolism level was relatively high in depletion T cells and relatively low in functional T cells (Fig. 1M). The hypoxia metabolism level of was relatively high in depletion T cell and functional T cell clusters (Fig. 2A). Tregs also were divided into two subclusters (Fig. 2B). As shown in Fig. 1, cluster 0 Treg cells were defined as Interleukin 10 (IL10) +Tregs, according to the highly expression of IL10. Cluster 0 Treg cells were defined as CD52 +Tregs (Fig. 2C), according to the high expression level of CD52. The level of lactic acid metabolism was relatively high (Fig. 2D), level of glycolysis metabolism was relatively low (Fig. 2E), and level of hypoxia metabolism had a high degree of heterogeneity in Tregs (Fig. 2F).

3.2 Lactic Acid Metabolism and Communication Characteristics of OS Malignant Cell Subclusters

Previous studies have shown that lactate regulates biological functions of tumor cells and multiple types of immune cells in the tumor microenvironment through histone lactylation [36]. Therefore, we also examined the expression profiles of histone lactylation-related regulatory

genes, including Histone Deacetylase 1 (HDAC1) and Histone Deacetylase 3 (HDAC3) [37]. The results showed that HDAC1 expression level was relatively high in endothelial cells, whereas HDAC3 expression level was relatively high in Tregs (Fig. 3A). To further observe the heterogeneity of lactic acid metabolism in tumor cells, we first extracted tumor cells and divided them into five subclusters (Fig. 3B), combined with the expression of cell markers and singleR results (Fig. 3C), OS cluster 1 was defined as TIMP3+MMP13+ cluster, OS cluster 2 was defined as MMP9+HMGAI1+ cluster, OS cluster 3 was defined as BIRC5+STMN1+ cluster, OS cluster 4 was defined as SPARCL1+NDUFA4L2+ cluster, and OS cluster 5 was defined as CTSK+CD68+ cluster. Additionally, the results of pseudo-differentiation analysis showed that OS cluster 1 was a relatively low differentiation cluster. The OS cluster 2 was defined as a relatively highly differentiated cluster (Fig. 3D,E). The overall evaluation results for lactic acid-related genes showed that in cluster 2 the overall level was higher, whereas in cluster 1, the overall level was low (Fig. 3F). Further, a pseudo-differentiation heatmap showed that multiple lactic acid metabolism-related genes, including *PER2*, *BCKDHA*, *ETHE1*, *HMGCL*, *MPC1*, *LYRM4*, *PNKD*, and *SOD1*, were highly expressed at the end stages of differentiation, while genes including *SCU*, *NDUFS8*, *CHCHD10*, *CLPB*, *NDUFA10*, and *NDUFAF4* were highly expressed at the early stage of differentiation (Fig. 3G). In addition, the distribution of lactic acid metabolism-related genes on the chromosomes was observed. The results showed that these genes were evenly expressed on each chromosome, and relatively more expressed on chromosomes of 1, 2, and 12 (Fig. 3H). Subsequently, we conducted an intercellular communication analysis targeting lactate metabolism-related genes. The results showed that the top 20 most relevant cytokines targeted lactate metabolism-related genes in cluster 2 OS cells (Fig. 3I). Interestingly, *MIF* was universally highly correlated with all the target genes (Fig. 3J). In addition, the dot plot results also showed a higher expression level of *MIF* gene in OS cluster 2; the results also show that the expression level of *TIMP1* was higher in OS cluster 1, and that the expression levels of *ITGAM*, *CXCL2*, *PTDSSI*, *PTPRC*, and *MIF* were also higher in OS cluster 2 (Fig. 3K).

3.3 Lactic Acid Metabolism-Related Molecular Subgrouping of OS Samples

Based on the high heterogeneity in lactate metabolism among different cell clusters at the single-cell level, we further used lactate metabolism-related genes for the unsupervised molecular typing of OS transcriptome samples and divided them into three subtypes, two of which were determined because a group with a small sample size was eliminated (Fig. 4A–C). We further verified the results of the single cell analysis by analyzing the infiltration of various cell types in transcriptome samples by firstly extracting markers of various cell subtypes including OS clus-

ter 1, OS cluster 5, Tregs, and T cells (Fig. 4D–J). Functional enrichment result of OS cluster included ribosomal large subunit, ribosomal RNA (rRNA) metabolic process, rRNA processing, cellular respiration, oxidative phosphorylation, cytoplasmic translation, aerobic respiration, ribosome biogenesis, ribonucleoprotein complex, Adenosine triphosphate (ATP) metabolic process, mitochondrial matrix, large ribosomal subunit, collagen-containing, extracellular matrix, inner mitochondrial membrane, protein complex, cell-substrate junction, focal adhesion, ribosome, mitochondrial inner membrane, electron transfer activity, ribonucleoprotein complex binding, oxidoreduction-driven active, transmembrane transporter activity, proton transmembrane transporter activity, cadherin binding, unfolded protein binding, and collagen binding. These marker genes were utilized for ssGSEA to further compare the tissue content of various cell types in different molecular subtypes of OS samples, and the results show that cluster 2 exhibited significantly higher proportions of OS cluster 4 cells, OS cluster 5 cells, OS cluster 2 cells, and T cells, whereas the abundance of OS cluster 3 cells and Tregs was relatively greater in cluster 1 (Fig. 4K). To further explore the molecular characteristics between clusters, we comprehensively assessed the differences in the immune microenvironment by conducting an immune infiltration analysis between lactate metabolism clusters 1 and 2. Cluster 2 exhibited significantly higher proportions of multiple types of immune cells, including activated dendritic cells, eosinophils, gamma delta T cells, immature B cells, myeloid-derived suppressor cells (MDSCs), natural killer cells (NK cells), plasmacytoid dendritic cells, regulatory T cells, T follicular helper cells, and type II T helper cells (Fig. 4L). Thus, we defined cluster 2 as immune-hot cluster and cluster 1 as immune-cold cluster. GSVA was consistently used to further explore the functional differences associated with cluster-specific differentially expressed genes (DEGs) between the two clusters. Furthermore, the GSVA enrichment results showed significant functional differences between the two groups. Specifically, the GSVA-GO results showed that differentially enriched functions included messenger RNA (mRNA) 3-end processing, ruffle membrane, positive regulation of organelle organization, regulation of supramolecular fiber organization, negative regulation of cytoskeleton organization, phospholipid translocating ATPase complex, structural constituent of nuclear pore, nuclear export signal receptor activity, positive regulation of RNA splicing, regulation of clathrin-dependent endocytosis, regulation of receptor-mediated endocytosis, and regulation of endocytosis (Fig. 4M). The GSVA-KEGG results showed that the differentially enriched functions included nitrogen metabolism, Fc gamma R-mediated phagocytosis, ErbB signaling pathway, adherens junction, small cell lung cancer, inositol phosphate metabolism, endocytosis, sulfur metabolism, histidine metabolism, primary bile acid biosynthesis, biosynthesis of unsaturated fatty acids, and oxidative phosphorylation (Fig. 4N).

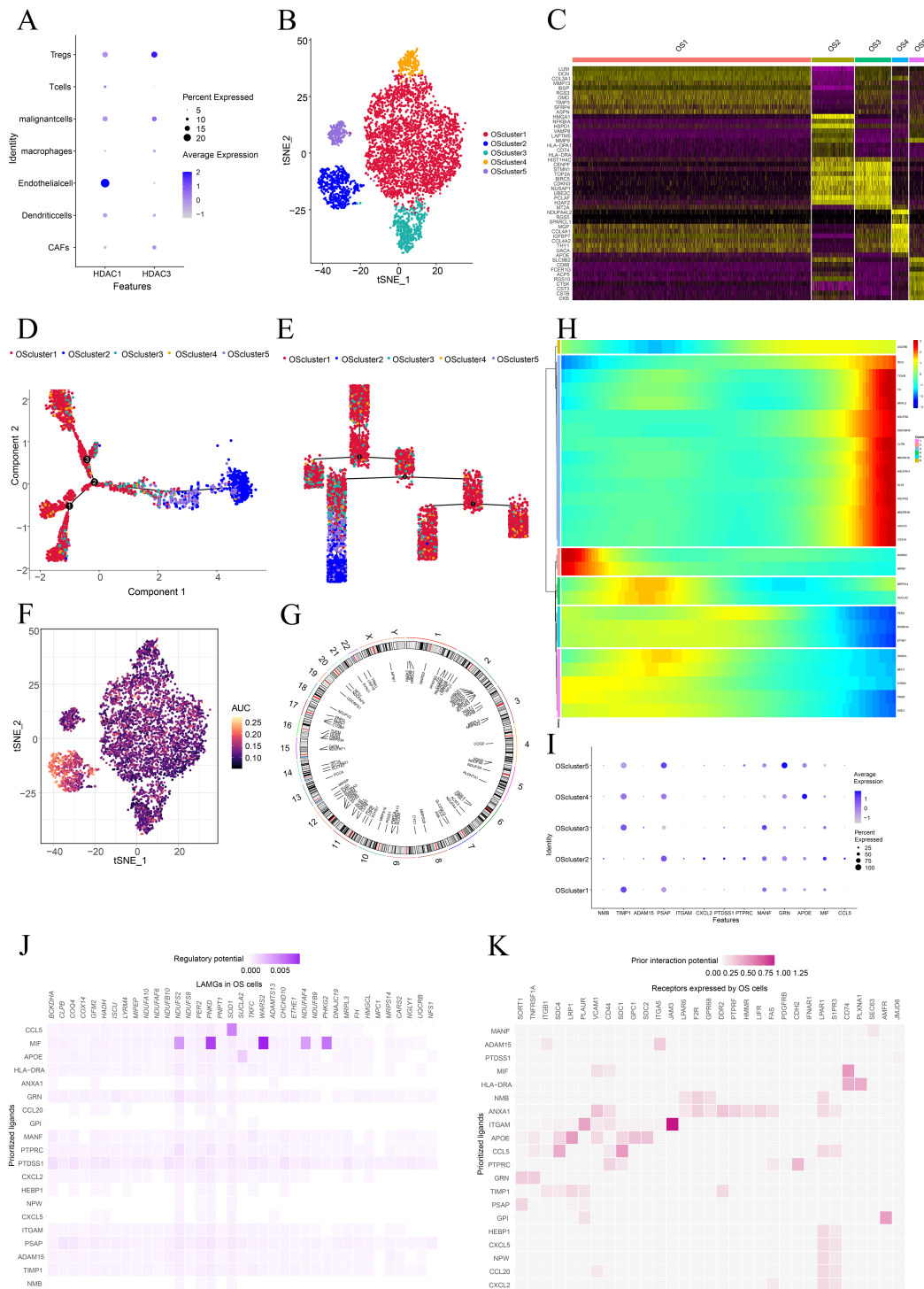


Fig. 3. Lactic acid metabolism characteristics of osteosarcoma (OS) malignant cell subclusters. (A) Dot plots shows the lactylation-related regulatory genes expressed across the osteosarcoma sample. The size of dots indicates the proportion of cells expressing the marker, the spectrum of color represents the mean expression levels of the markers. (B) t-SNE plot shows the five OS subclusters. (C,D) Cell trajectory plot shows the five OS subclusters. (E) Heatmap shows the top differentially expressed genes in OS subclusters. (F) t-SNE plot shows the Lactate Metabolism Genes (LAMGs) from the osteosarcoma sample. (G) Pseudo-temporal differentiation locus of the LAMG expression in OS clusters. (H) Chromosome locus analysis of genes in LAMGs. (I) Heatmap of ligand-target LAMG interactions in the niche cell-OS cluster 2 cell communication. (J) Top ligand-receptor interaction pairs in the niche cell-OS cluster 2 cell communication. (K) Dot plots show the LAMG interaction-related genes expressed across the osteosarcoma sample.

3.4 Construction of LRG-Based OS Prognostic Model

To identify the high diagnostic value of LAMGs, two proven machine learning models, the RF and SVM mod-

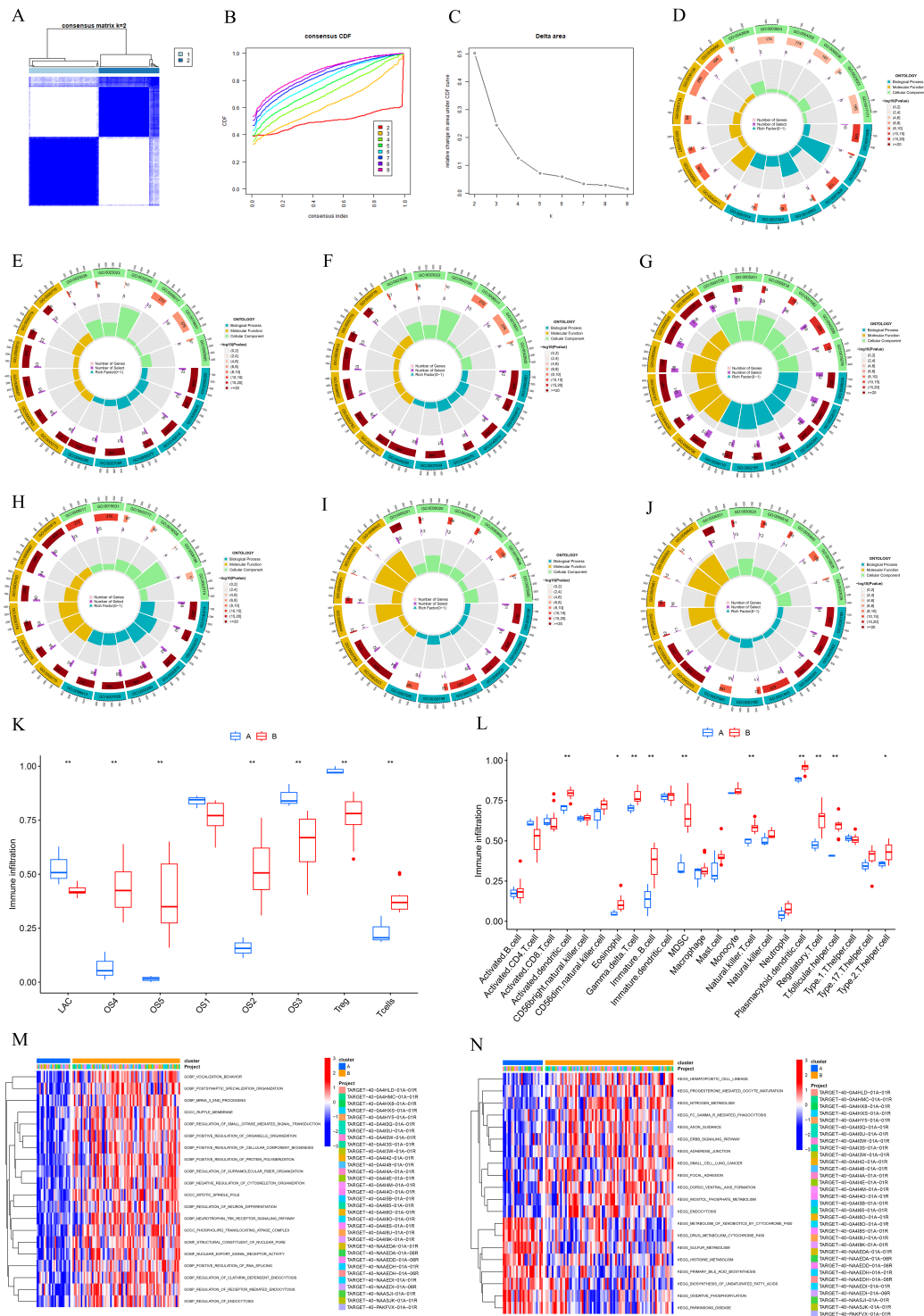


Fig. 4. Clustering different microenvironment subtypes of osteosarcoma based on LAMGs. (A–C) Consensus clustering identified three distinct clusters of OS with different LAMG expression patterns. (D) Circle plot of Gene Ontology (GO) pathway activities of the T cells cluster markers. (E) Circle plot of GO pathway activities of the Tregs cluster markers. (F) Circle plot of GO pathway activities of the OS cluster 1 markers. (G) Circle plot of GO pathway activities of the OS cluster 2 markers. (H) Circle plot of GO pathway activities of the OS cluster 3 markers. (I) Circle plot of GO pathway activities of the OS cluster 4 markers. (J) Circle plot of GO pathway activities of the OSCs subcluster 5 markers. (K) Single-sample gene set enrichment analysis (ssGSEA) scoring and differential analysis of marker genesets. (L) ssGSEA scoring and differential analysis of 22 immune cells. (M) GSEA-GO analysis of LAMG clusters. (N) GSEA-KEGG analysis of LAMG clusters. “*” represents for p value under 0.05 and “**” represents for p value under 0.01. GSEA, Gene Set Variation Analysis; KEGG, Kyoto Encyclopedia of Genes and Genomes; OSC, osteosarcoma cells.

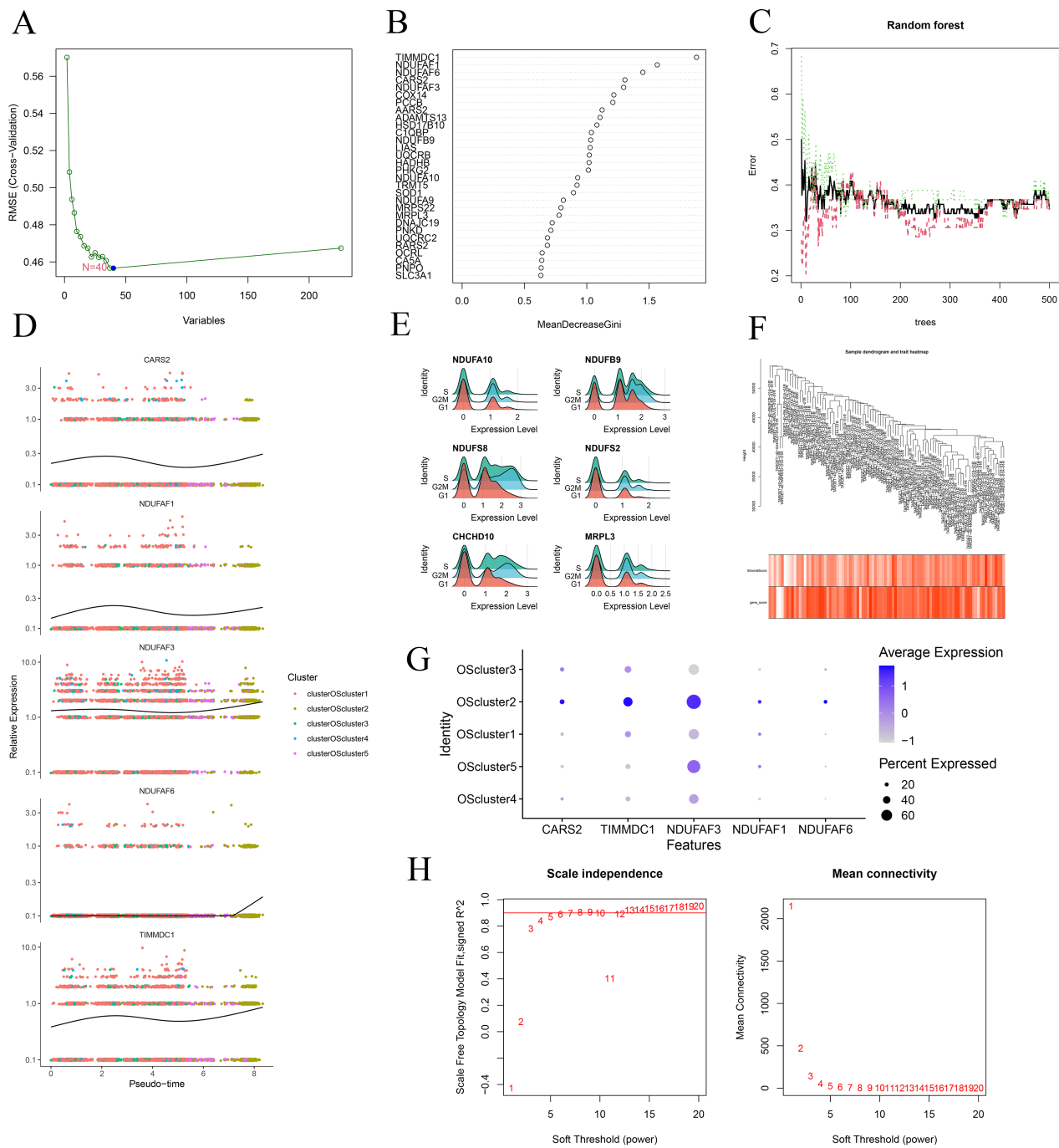


Fig. 5. Screening of the hub genes. (A) SVM-RFE screening of candidate diagnostic genes. (B,C) Error graph of the random forest (RF) models. (D) Pseudo-temporal differentiation locus of the hub genes in OS. (E) The RidgePlot illustrating the correlation between the hub gene expression and cell cycle. (F) Dot plots shows the hub gene expression across from the OS clusters. (G) Sample clustering heatmap of weighted gene coexpression network analysis (WGCNA) analysis. (H) Scale independence analysis of WGCNA. SVM, support vector machine; RFE, recursive feature elimination; RMSE, root mean square error.

els, were utilized based on the expression profiles of the OS cohort. The results show that we constructed an SVM prediction model that included 40 LAMGs (Fig. 5A) and an RF prediction model with LAMG expression of *TIMMDC1*, *NDUFAF1*, *NDUFAF6*, *CARS2*, and *NDUFAF3* (Fig. 5B,C). Subsequent pseudo-time trajectory analysis showed that LAMGs, including *NDUFAF6* and *NDUFAF3*,

were highly expressed at the end stage of OS differentiation (Fig. 5D). The cell cycle-related expression analysis results showed a relatively low expression level of *NDUFS8* in the G1 phase, but it was high in the G2M and S phases (Fig. 5E). Expression levels of *CARS2* and *NDUFAF6* were relatively high in OS cluster 2 (Fig. 5F). Moreover, all were used to construct the WGCNA (Fig. 5G,H, and Fig. 6A–C). The

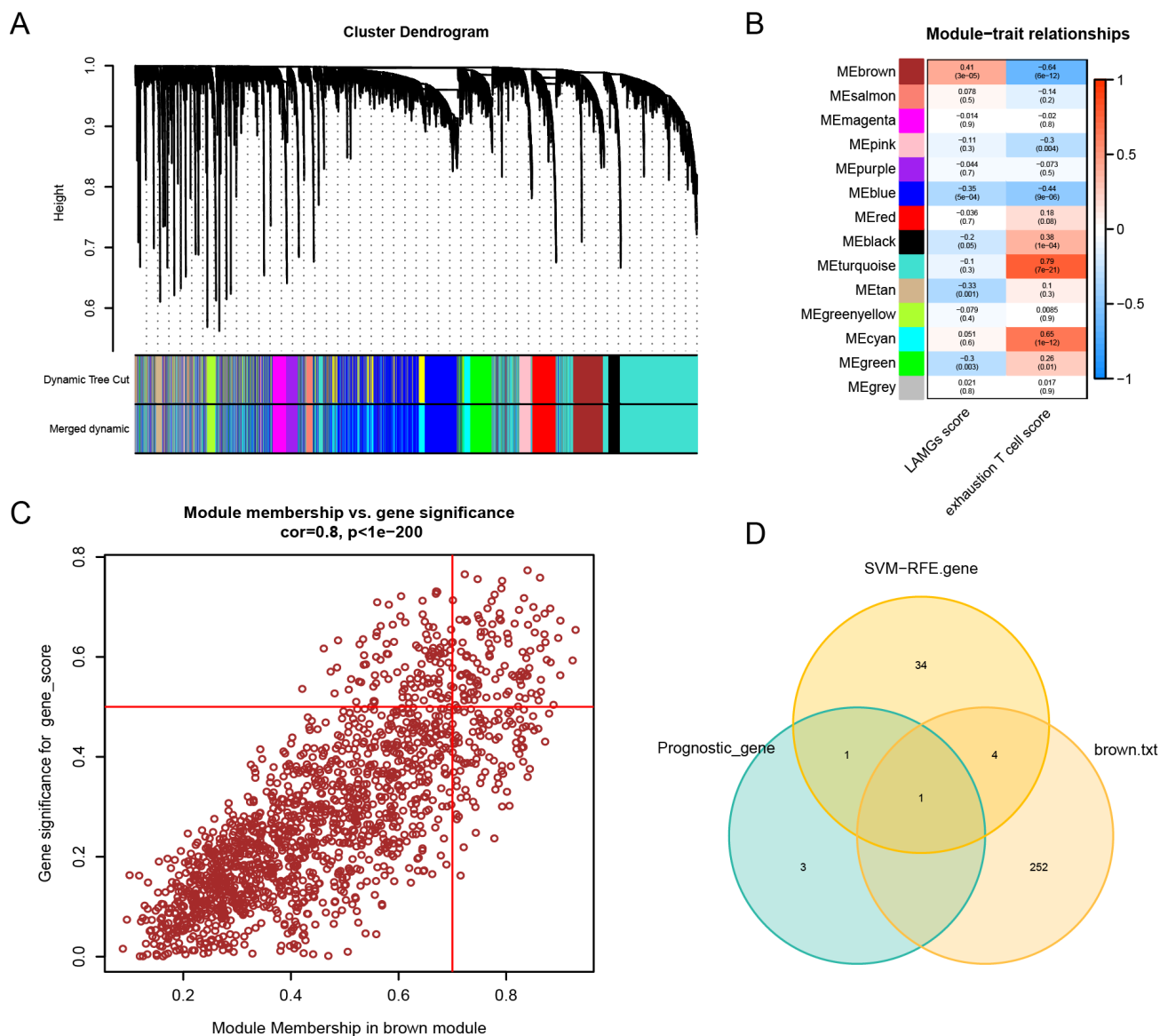


Fig. 6. WGCNA analysis. (A) Merged dynamic analysis of WGCNA. (B) Module trait of WGCNA analysis. (C) Screening of genes in brown module. (D) The Venn diagram displays the intersection of the results of the three gene sets.

network was constructed using a soft threshold $\beta=9$, and 14 modules were identified (Fig. 4A). Among these modules, the brown module showed the most significant correlation with lactic acid metabolic scores ($\text{cor} = 0.41, p < 0.01$) and exhaustion T cell scores ($\text{cor} = -0.64, p < 0.01$), and was considered the key module in this study (Fig. 4B). Combined with the candidate hub gene screening thresholds for GS and MM, 257 genes were identified for further analysis (Fig. 4C). Next, we intersected the gene set obtained from the machine learning methods with the WGCNA gene set (Fig. 6D) and obtained the key gene, NADH:Ubiquinone Oxidoreductase Complex Assembly Factor 6 (*NDUFAF6*), for further analysis.

3.5 Screening and Characterization of the Key Gene, *NDUFAF6*

We validated the correlation between hub genes and immune cell infiltration, revealing that the expression of *NDUFAF6* was negatively correlated with monocytes ($R = -0.29, p = 0.0031$; Fig. 7A,B). Furthermore, the correlation between *NDUFAF6* and potential drugs was validated. Chelerythrine, ifosfamide, methylprednisolone, nelarabine, PX-316, ribavirin, and vorinostat were screened as potential drugs targeting *NDUFAF6* in OS (Fig. 7C-I). Afterwards, a differential functional annotation analysis was performed between the *NDUFAF6*-high and *NDUFAF6*-low expression groups of the transcriptome data. The top GSEA-GO enrichment analysis results included negative regulation of map kinase activity, regulation of receptor recycling, renal system vasculature development, ribosomal large subunit assembly, substantia nigra development, cell body

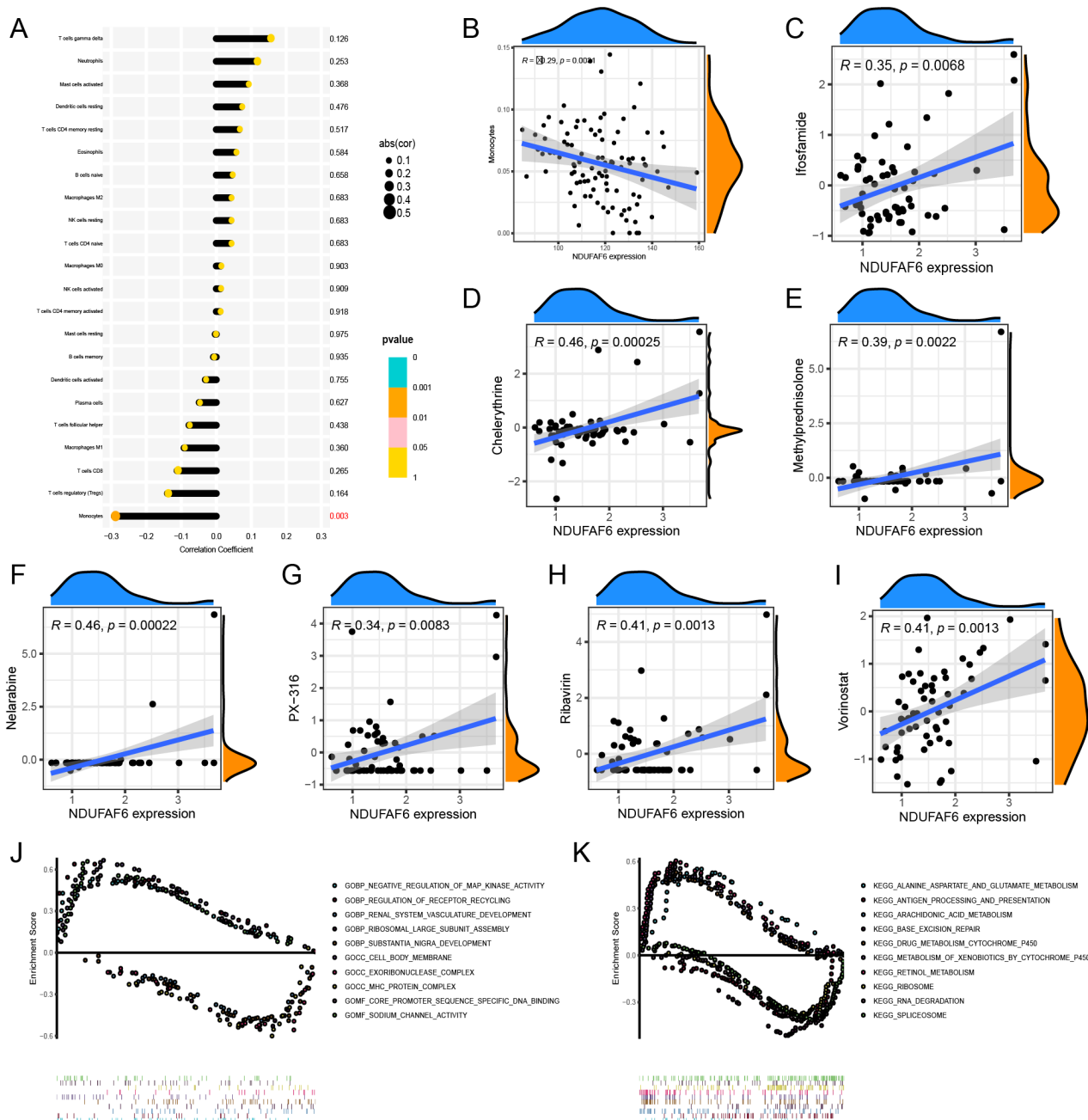


Fig. 7. Immune, drug sensitive, and function enrichment analysis of NDUFAF6. (A,B) Correlation analysis between *NDUFAF6* and infiltration scores of immune cells. (C–I) Correlation analysis between *NDUFAF6* and drug sensitive scores. (J) GSEA-GO analysis of *NDUFAF6*. (K) GSEA-KEGG analysis of *NDUFAF6*. GSEA, gene set enrichment analysis.

membrane, exoribonuclease complex, MHC protein complex, sequence-specific DNA binding of core promoter, and sodium channel activity (Fig. 7J). The top GSEA-KEGG enrichment analysis results included alanine aspartate and glutamate metabolism, antigen processing and presentation, arachidonic acid metabolism, base excision repair, drug metabolism, cytochrome p450, xenobiotic metabolism by cytochrome p450, retinol metabolism, ribosomes, RNA degradation, and spliceosomes (Fig. 7K).

3.6 *In vitro* Lactate or siNDUFAF6 Treatment Regulates OS Cells Survival

To determine whether lactate expression and exogenous siNDUFAF6 were involved in the OS cells survival, lactate and siNDUFAF6 were separately treated with lactate 143B cells (Fig. 8). The CCK-8 assay showed that the viability of 143B cells decreased after siNDUFAF6 treatment and decreased under LA+siNDUFAF6 treatment (Fig. 8A,B). Transwell assays showed that cell invasiveness was significantly decreased in the LA+siNDUFAF6 treatment group (Fig. 8C,D). We further examined the role

of *NDUFAF6* in metabolic reprogramming under the condition of TME by evaluating the changes of Extracellular Acidification (ECAR) parameters. The results showed that the glycolytic ability and glycolytic reserve of osteosarcoma cells decreased after the siNDUFAF6 treatment (**Supplementary Fig. 1A**). qRT-PCR results indicate that the *NDUFAF6* and *TIMMDC1* expression levels significantly decreased after LA+siNDUFAF6 treatment (Fig. 8E), it is also find that the expression of *NDUFAF6* in OS cells reduced after adding chelerythrine (**Supplementary Fig. 1B**).

3.7 Higher Expression Level of *NDUFAF6* in Tumors in OS Patients and Lower Immune Score Group

The *NDUFAF6* expression level in each patient was determined using qRT-PCR and IHC. The expression level of *NDUFAF6* in OS tissue group and lower immune score group were respectively higher than that in the adjacent tissue group (nine cases, Fig. 8F) and higher immune score group (five cases, Fig. 8G). IHC results also confirmed that the protein expression levels of *NDUFAF6* OS tissue group were respectively higher than that in the adjacent tissue group (**Supplementary Fig. 1C**).

4. Discussion

Metabolic reprogramming is a hallmark of cancer cells and has recently been identified as a key factor in tumor progression [38]. However, the metabolic profile of OS remains unclear [39]. Various metabolic markers, including elaidic acid, docosahexaenoic acid, and octadecanoic acid, were expressed differentially between OS lung metastases development and nonmetastatic state, as a consequence of hypoxia and the shift from consumption of carbohydrates and amino acids to lipids [40], concomitantly, the levels of glucose, glucose phosphate, and gluconolactone were decreased, while uridine and uracil increased during the metastatic phase as a consequence of metabolic shunting towards ribose [41]. OS also illustrates the role of glutathione pathway downregulation and high hypoxic levels during metastasis [42]. In this study, we found that the genes expression levels related to lactic acid, fatty acid, glycolic metabolism, butyric acid metabolism, and glycolysis metabolism were relatively high in malignant OS cells. This is consistent with previous findings that glycolysis promotes tumor invasion and metastasis [43]. cholesterol metabolism and its metabolites can also promote tumor invasiveness [44]. Butyrate affects the metabolism of OS cells by regulating cell differentiation and the expression of anti-inflammatory mediator-related genes [45]. At present, increasing evidence shows that multiple types of immune cells in the tumor microenvironment are similar to tumor cells, and the abnormal metabolism of cells is caused by the combined action of various factors that have a profound influence on tumor immunity [46]. Our results show that T cells in OS tissues are composed of activated T cells and exhausted T cells. These two subtypes show distinct

metabolic profiles, including lactic acid, glycolysis, and hypoxia metabolism, indicating that lactic acid metabolism is highly involved in the biological processes of activation and exhaustion of T cells and that lactic acid dampens the function of T cells by suppressing T cell cytokine production and restraining the redox system of T cells [47]. Hypoxic metabolism also shows high heterogeneity in Treg cells, and it has been proven that hypoxia favors Tregs in terms of differentiation, suppressive recruitment, and function [48].

Similar to other fatty acids, L-lactic acid can also form the corresponding fatty acyl-CoA and L-lactyl-CoA. Zhao *et al.* [49] first reported that lactic acid is an important epigenetic regulatory molecule; histones can undergo lactate modification K (L-la) and regulate the expression of genes related to macrophage polarization during immune activation [50,51]. Previous studies have also examined the potential regulatory effects of HDACs on lactate modification and found that Class I HDACs (HDAC 1-3) are the most effective lysine lactate modification erasers, in which HDAC1 and 3 play a role in cell de-lactate activity [37]. Our results also revealed highly heterogeneous expression of HDAC1 and 3 in the OS microenvironment. Our results on tumors and tumor-infiltrating T cells suggest that lactic acid metabolism in OS and lactic acid itself in the microenvironment may play an important role in the progression of OS. The role of lactic acid in oncogenesis and progression has long been underestimated because it is primarily considered as a waste product of glycolysis or a marker of poor prognosis [42,52]. In recent years, lactic acid has been found to play a key role in promoting tumor growth, angiogenesis, immune escape, invasion, metastasis, metabolic regulation, and cell interactions in the TME [53,54]. For example, tumor cells produced lactic acid can be secreted into the extracellular environment to promote cancer progression [7]. The proton-coupled lactate efflux system in tumor and tumor-associated stromal cells regulates survival signaling and prevents immune surveillance of tumor cells to promote tumor progression. Extracellular acidosis inhibits T cell-mediated immunity, and neutralization of tumor acidity may enhance the antitumor effects of immunotherapy [55]. To further explore the key role of lactic acid metabolism in OS cells, we divided malignant OS cells into five subgroups. OS cluster 2 had significantly high glycolysis and lactic acid metabolism levels, and the results of marker genes functional enrichment in OS cluster 2 showed that functions including mitochondrial matrix, inner mitochondrial membrane, and oxidoreduction-driven activity were highly enriched, suggesting that lactic acid metabolism is related to the functions of mitochondrial metabolism. The high metabolic heterogeneity within solid tumors may be caused by vascular integrity and proximity to the vasculature that transports oxygen and nutrients [56]. Well-vascularized tumor subregions can access a variety of nutrients, whereas poorly perfused areas utilize glucose as their main carbon source [57]. Lactic acid metabolism can affect the oxidation state of cells, leading to the conversion

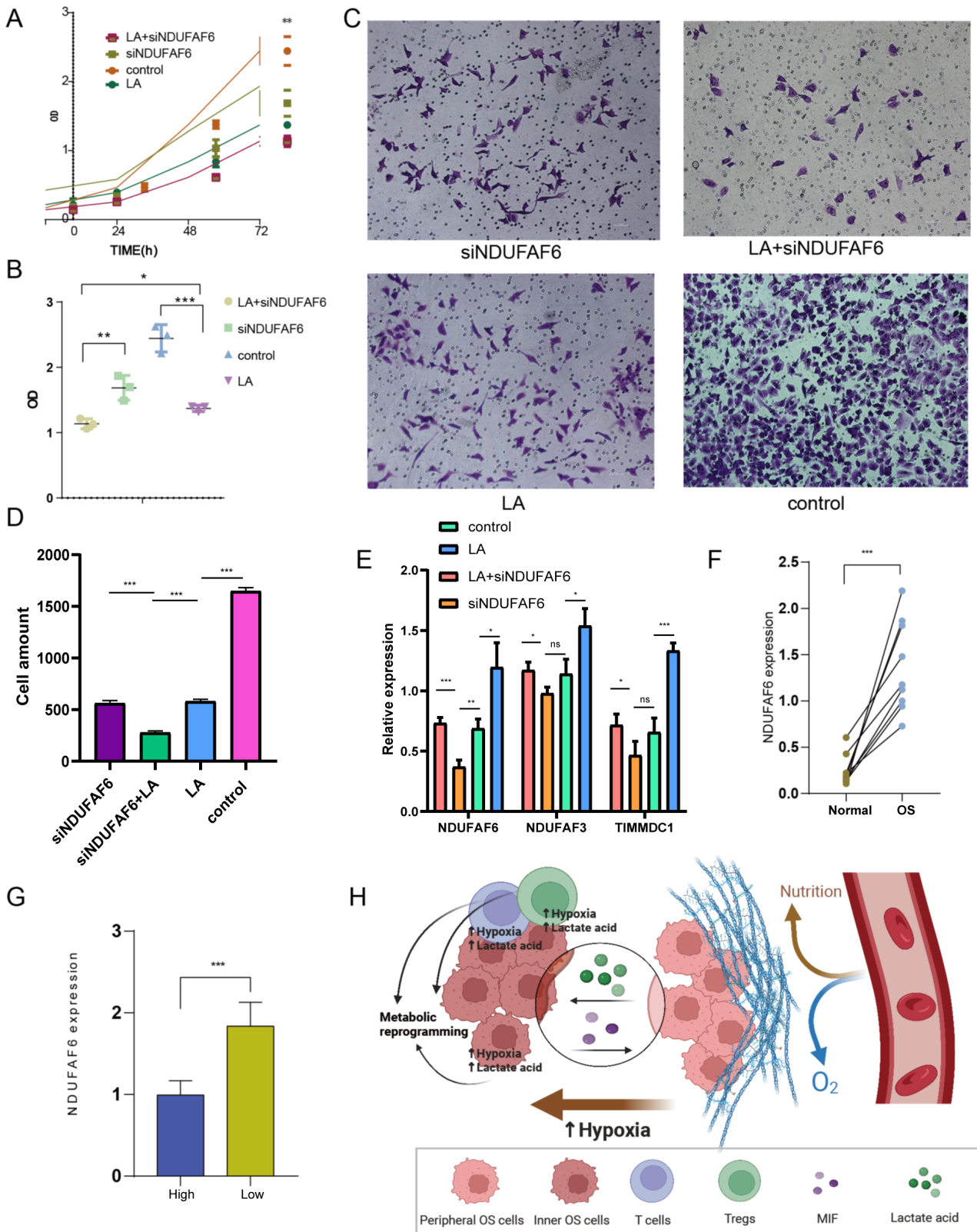


Fig. 8. *In vitro* and patient experiment. (A,B) 143B cell viability after treatment with siNDUFAF6 or LA. (C,D) Transwell experiment treatment with siNDUFAF6 or LA. (E) qRT-PCR validate the expression of *NDUFAF6*, *TIMMDC1*, and *NDUFAF3* with different treatment. (F) The *NDUFAF6* expression level in OS and normal tissue. (G) *NDUFAF6* expression levels in different patient groups. (H) Mechanism diagram. “*” represents for *p* value under 0.05, “**” represents for *p* value under 0.01, “***” represents for *p* value under 0.001, and “ns” represents for *p* value over 0.05. qRT-PCR, quantitative reverse transcriptase polymerase chain reaction. LA, lactic acid.

of glucose to pentose phosphate pathway and the biosynthesis of hexosamine. The innermost cells of the tumor are in a state of high oxygen deficiency and high lactic acid concentration, resulting in high lactic acid metabolism in the tumor cell population in this region. Therefore, we suggest OS cluster 2 as the cell cluster in this position. In addition, research has shown that tumor cells within tumors cooperate in a metabolic “symbiosis”. For example, tumor cells in hypoxic regions consume glucose by anaerobic glycolysis and release lactic acid, which is then utilized by tumor cells in adjacent oxygen-containing tumor regions to fuel the tricarboxylic acid cycle and form a biological process called lactate shuttles [58]. We also found that amino acid levels in the core of the tumor were higher than those in the periphery, and it is assumed that peripheral cancer cells release these amino acids as an energy source for internal tumor cells [57]. The role of cytokines in the regulation of tumor metabolism has been gradually discovered, for example, IL4 and IL13 in pancreatic cancer promote glucose utilization. Our research suggests that MIF plays a crucial role in the metabolic communication of OS cells. MIF, as an autocrine growth factor, has been discovered to be involved in cholesterol metabolism in a variety of diseases. The expression of MIF has a vital influence on adipocyte metabolism and immune regulation [59]. MIF is involved in the regulation of malignant phenotypes in various types of cancers by activating a variety of signaling pathways. An abnormal increase in MIF expression level improves the migration, proliferation, and invasiveness of gastric, breast, and lung cancer cells [60–63]. CXCL2/MIF-CXCR2 signaling activation in bladder cancer cells intensifies the accumulation and expansion of MDSC in the TME [64].

GSVA results showed that differentially enriched functions include nitrogen metabolism and the ErbB signaling pathway. The metabolites of glycolytic metabolism on the one hand have basic functions as major energy and biosynthetic sources, and on the other hand are also involved in the regulation of immune cell reprogramming metabolic pathways to meet energy and biosynthetic requirements during immune cell activation. Various lymphocytes in tumor cells, including inflammatory M1 macrophages, transition from oxidative phosphorylation to glycolysis to adapt to the TME [65]. Oncogene *ErbB2* has been shown to enhance the Warburg effect by activating heat shock factor 1 and regulating lactate dehydrogenase A [49]. *ErbB2* overexpression increases glucose uptake and lactic acid production [66]. To further explore the molecular characteristics between clusters, we comprehensively assessed the differences in the immune microenvironment by conducting an immune infiltration analysis between lactate metabolism cluster 1 and cluster 2. Cluster 2 exhibited significantly higher proportions of multiple types of immune cells, including activated dendritic cells, eosinophils, gammadelta T cells, immature B cells, MDSCs, NK cells, plasmacytoid dendritic cells, regulatory T cells, T follicular helper cells, and type II T helper cells.

Thus, we defined cluster 2 as immune-hot cluster and cluster 1 as immune-cold cluster. We further validated the results of the single-cell analysis by analyzing the infiltration of various cell types in the transcriptome samples and show that cluster 2 exhibited significantly higher proportions of OS cluster 4 cells, OS cluster 5 cells, OS cluster 2 cells, and T cells, whereas the abundance of OS cluster 3 cells and Tregs was relatively greater in cluster 1. These results suggest that lactate metabolism is involved in the TME regulation. Insights into LAMGs may facilitate the discovery of the mechanisms regulating tumor immunity and pave the way for future TME studies. Although numerous studies support a relationship between tumor lactate metabolism and immune escape in the tumor microenvironment [23], the specific molecules responsible for this relationship have not been identified. Genes including *TIMMDC1* and *NDUFAF1* were screened as hub genes. *TIMMDC1* (*C3orf1*) is a four-pass membrane protein located in the mitochondrial inner membrane. It is suggested that *TIMMDC1* is associated with multiple members of mitochondrial complex I assembly factors, reduced mitochondrial respiration, reduced glycolysis activity, and the AKT/GSK3 β / β -catenin signaling pathways [67]. In T cells, the inhibition of mitochondrial electron transport complex I assembly by knocking down the chaperone *NDUFAF1* blocked ROS production. Complex I-derived ROS are converted into hydrogen peroxide signals by mitochondrial superoxide dismutase, and the inhibition of complex I assembly by *NDUFAF1* knock-down prevents activation-induced T cell death [68].

Our *in vitro* expression results showed that knock-down of *NDUFAF6* decreased OS cell viability and invasiveness. It is reported that mitochondria can actively migrate to certain subcellular regions with high energy requirements along cytoskeleton filaments and undergo mitochondrial fission to meet the needs of cell migration, invasion and cell proliferation, so we assume that *NDUFAF6* can enhance the invasion and growth ability of osteosarcoma cells through these mechanisms [69]. The patient experiment showed that expression level of *NDUFAF6* is higher in OS tissue. The expression level of *NDUFAF6* significantly correlated with the monocyte infiltration level. One subtype of monocytes, also known as patrolling monocytes (PMos), has been recognized as potentially relevant to OS; unlike classical monocytes that promote tumorigenesis and metastasis, nonclassical PMos have been shown to decrease breast metastasis [70]. Although there is limited research on how *NDUFAF6* regulates immune processes in OS, our results suggest that molecules involved in lactic acid metabolism and immune processes in OS may be potential targets for the development of new therapeutic strategies. Lactate accumulation has been shown to be associated with increased cancer resistance and malignancy [71]; thus, screening drugs that target lactate metabolism for combination therapy has a key potential role in the efficacy of chemotherapy for OS. We identified chelerythrine and vorinostat as potential drugs

that target *NDUFAF6*. Chelerythrine, an IL-2 inhibitor, selectively inhibits the interaction between IL-2 and IL-2R α by directly binding to IL-2 and preventing the transformation of infantile CD4 T cells into CD4CD25Foxp3 Treg cells. The combination of chelerythrine and PD-1 inhibitors increases the antitumor activity in melanoma mice [72]. The histone deacetylase inhibitor suberanilohydroxamic acid (vorinostat) is a clinically effective drug against mutant TP53 tumor cells. Vorinostat and PENAO synergistically reduce the viability of neuroblastoma cells and induce apoptosis independent of the TP53 state. The combination of vorinostat and PENAO significantly delays tumor progression in preclinical neuroblastoma mice [73]. Functional enrichment analysis of *NDUFAF6* showed that the potential functions of *NDUFAF6* include MHC protein complex, glutamate metabolism, drug metabolism cytochrome p450, antigen presentation, metabolism of xenobiotics by cytochrome p450, and retinol metabolism, ribosome spliceosome, which is consistent with the finding that *NDUFAF6* is involved in abnormal lactate metabolism and tumor immunity associated with OS.

5. Conclusions

Lactic acid metabolism patterns in OS revealed metabolic reprogramming phenotypes relevant to the tumor microenvironment, and *NDUFAF6* was identified as an LRG biomarker (Fig. 8H).

Availability of Data and Materials

The datasets generated and analyzed during the current study are available from the corresponding authors upon reasonable request.

Author Contributions

LW, XD, JL and XL designed the research study. LW, XD and LX performed the research. YL provided help and advice on methodology. LW, XD, LX and XZ analyzed the data. LW, XD, XZ, JL and XL wrote the manuscript. All authors contributed to editorial changes in the manuscript. All authors read and approved the final manuscript. All authors have participated sufficiently in the work to take public responsibility for appropriate portions of the content and agreed to be accountable for all aspects of the work in ensuring that questions related to its accuracy or integrity.

Ethics Approval and Consent to Participate

The experiments were performed under a project license granted by the Ethics Committee of Honghui Hospital, Xi'an Jiaotong University (protocol code 202303051). Informed consent was obtained from all patients in this study.

Acknowledgment

Not applicable.

Funding

This research was funded by the Beijing Municipal Science & Technology Commission, Administrative Commission of Zhongguancun Science Park to XL, grant number Z191100007619023 and the National Natural Science Foundation of China to XL, grant number: 81972103, 82372451.

Conflict of Interest

The authors declare no conflict of interest.

Supplementary Material

Supplementary material associated with this article can be found, in the online version, at <https://doi.org/10.31083/j.fbl2902083>.

References

- [1] Choi JH, Ro JY. The 2020 WHO Classification of Tumors of Bone: An Updated Review. *Advances in Anatomic Pathology*. 2021; 28: 119–138.
- [2] Weiss A, Houry JD, Hoffer FA, Wu J, Billups CA, Heck RK, *et al.* Telangiectatic osteosarcoma: the St. Jude Children's Research Hospital's experience. *Cancer*. 2007; 109: 1627–1637.
- [3] Kansara M, Teng MW, Smyth MJ, Thomas DM. Translational biology of osteosarcoma. *Nature Reviews. Cancer*. 2014; 14: 722–735.
- [4] Jaffe N, Frei E, 3rd, Traggis D, Bishop Y. Adjuvant methotrexate and citrovorum-factor treatment of osteogenic sarcoma. *The New England Journal of Medicine*. 1974; 291: 994–997.
- [5] Kager L, Zoubek A, Pötschger U, Kastner U, Flege S, Kempf-Bielack B, *et al.* Primary metastatic osteosarcoma: presentation and outcome of patients treated on neoadjuvant Cooperative Osteosarcoma Study Group protocols. *Journal of Clinical Oncology: Official Journal of the American Society of Clinical Oncology*. 2003; 21: 2011–2018.
- [6] Bielack SS, Kempf-Bielack B, Delling G, Exner GU, Flege S, Helmke K, *et al.* Prognostic factors in high-grade osteosarcoma of the extremities or trunk: an analysis of 1,702 patients treated on neoadjuvant cooperative osteosarcoma study group protocols. *Journal of Clinical Oncology: Official Journal of the American Society of Clinical Oncology*. 2002; 20: 776–790.
- [7] Yoshida GJ. Metabolic reprogramming: the emerging concept and associated therapeutic strategies. *Journal of Experimental & Clinical Cancer Research: CR*. 2015; 34: 111.
- [8] Kim J, DeBerardinis RJ. Mechanisms and Implications of Metabolic Heterogeneity in Cancer. *Cell Metabolism*. 2019; 30: 434–446.
- [9] Yang J, Ren B, Yang G, Wang H, Chen G, You L, *et al.* The enhancement of glycolysis regulates pancreatic cancer metastasis. *Cellular and Molecular Life Sciences: CMLS*. 2020; 77: 305–321.
- [10] Tanyi JL, Hasegawa Y, Lapushin R, Morris AJ, Wolf JK, Berchuck A, *et al.* Role of decreased levels of lipid phosphate phosphatase-1 in accumulation of lysophosphatidic acid in ovarian cancer. *Clinical Cancer Research: an Official Journal of the American Association for Cancer Research*. 2003; 9: 3534–3545.
- [11] Duan L, Pang HL, Chen WJ, Shen WW, Cao PP, Wang SM, *et al.* The role of GDF15 in bone metastasis of lung adenocarcinoma cells. *Oncology Reports*. 2019; 41: 2379–2388.
- [12] Peng X, Chen Z, Farshidfar F, Xu X, Lorenzi PL, Wang Y, *et al.* Molecular Characterization and Clinical Relevance of Metabolic

- Expression Subtypes in Human Cancers. *Cell Reports*. 2018; 23: 255–269.e4.
- [13] Li WV, Li JJ. An accurate and robust imputation method scImpute for single-cell RNA-seq data. *Nature Communications*. 2018; 9: 997.
- [14] Jagla B, Libri V, Chica C, Rouilly V, Mella S, Puceat M, *et al.* SCHNAPPs - Single Cell sHiNy APpLication(s). *Journal of Immunological Methods*. 2021; 499: 113176.
- [15] Aran D, Looney AP, Liu L, Wu E, Fong V, Hsu A, *et al.* Reference-based analysis of lung single-cell sequencing reveals a transitional profibrotic macrophage. *Nature Immunology*. 2019; 20: 163–172.
- [16] Browaeys R, Saelens W, Saeys Y. NicheNet: modeling intercellular communication by linking ligands to target genes. *Nature Methods*. 2020; 17: 159–162.
- [17] Wilkerson MD, Hayes DN. ConsensusClusterPlus: a class discovery tool with confidence assessments and item tracking. *Bioinformatics (Oxford, England)*. 2010; 26: 1572–1573.
- [18] Hänzelmann S, Castelo R, Guinney J. GSEA: gene set variation analysis for microarray and RNA-seq data. *BMC Bioinformatics*. 2013; 14: 7.
- [19] Taylor JMG. Random Survival Forests. *Journal of Thoracic Oncology: Official Publication of the International Association for the Study of Lung Cancer*. 2011; 6: 1974–1975.
- [20] Langfelder P, Horvath S. WGCNA: an R package for weighted correlation network analysis. *BMC Bioinformatics*. 2008; 9: 559.
- [21] Wei H, Du X, Zhao H, Sun P, Yang J. Propofol Regulates ER Stress to Inhibit Tumour Growth and Sensitize Osteosarcoma to Doxorubicin. *International Journal of Clinical Practice*. 2023; 2023: 3093945.
- [22] Patel AP, Tirosh I, Trombetta JJ, Shalek AK, Gillespie SM, Wakimoto H, *et al.* Single-cell RNA-seq highlights intratumoral heterogeneity in primary glioblastoma. *Science (New York, N.Y.)*. 2014; 344: 1396–1401.
- [23] Xia M, Wang S, Wang L, Mei Y, Tu Y, Gao L. The role of lactate metabolism-related lncRNAs in the prognosis, mutation, and tumor microenvironment of papillary thyroid cancer. *Frontiers in Endocrinology*. 2023; 14: 1062317.
- [24] Ren Z, Gao D, Luo Y, Song Z, Wu G, Qi N, *et al.* Identification of fatty acid metabolism-related clusters and immune infiltration features in hepatocellular carcinoma. *Aging*. 2023; 15: 1496–1523.
- [25] Ji K, Dou W, Zhang N, Wen B, Zhong M, Zhang Q, *et al.* Retinoic acid receptor gamma is required for proliferation of pancreatic cancer cells. *Cell Biology International*. 2023; 47: 144–155.
- [26] Liu L, Mo M, Chen X, Chao D, Zhang Y, Chen X, *et al.* Targeting inhibition of prognosis-related lipid metabolism genes including CYP19A1 enhances immunotherapeutic response in colon cancer. *Journal of Experimental & Clinical Cancer Research: CR*. 2023; 42: 85.
- [27] Luo Q, Zhou P, Chang S, Huang Z, Zeng X. Characterization of butyrate-metabolism in colorectal cancer to guide clinical treatment. *Scientific Reports*. 2023; 13: 5106.
- [28] Sun W, Jia C, Zhang X, Wang Z, Li Y, Fang X. Identification of Key Genes Related With Aspartic Acid Metabolism and Corresponding Protein Expression in Human Colon Cancer With Postoperative Prognosis and the Underlying Molecular Pathways Prediction. *Frontiers in Cell and Developmental Biology*. 2022; 10: 812271.
- [29] Qu H, Li X, Chen F, Zhang M, Lu X, Gu Y, *et al.* lncRNA PVT1 influences breast cancer cells glycolysis through sponging miR-145-5p. *Genes & Genomics*. 2023; 45: 581–592.
- [30] Norian LA, Rodriguez PC, O'Mara LA, Zabaleta J, Ochoa AC, Cella M, *et al.* Tumor-infiltrating regulatory dendritic cells inhibit CD8⁺ T cell function via L-arginine metabolism. *Cancer Research*. 2009; 69: 3086–3094.
- [31] Hinshaw DC, Benavides GA, Metge BJ, Swain CA, Kammerud SC, Alsheikh HA, *et al.* Hedgehog Signaling Regulates Treg to Th17 Conversion Through Metabolic Rewiring in Breast Cancer. *Cancer Immunology Research*. 2023; 11: 687–702.
- [32] Liu B, Hu X, Feng K, Gao R, Xue Z, Zhang S, *et al.* Temporal single-cell tracing reveals clonal revival and expansion of precursor exhausted T cells during anti-PD-1 therapy in lung cancer. *Nature Cancer*. 2022; 3: 108–121.
- [33] Del Rio ML, de Juan CYD, Roncador G, Caleiras E, Álvarez-Esteban R, Pérez-Simón JA, *et al.* Genetic deletion of HVEM in a leukemia B cell line promotes a preferential increase of PD-1⁻ stem cell-like T cells over PD-1⁺ T cells curbing tumor progression. *Frontiers in Immunology*. 2023; 14: 1113858.
- [34] Nanjireddy PM, Olejniczak SH, Buxbaum NP. Targeting of chimeric antigen receptor T cell metabolism to improve therapeutic outcomes. *Frontiers in Immunology*. 2023; 14: 1121565.
- [35] Andrejeva G, Rathmell JC. Similarities and Distinctions of Cancer and Immune Metabolism in Inflammation and Tumors. *Cell Metabolism*. 2017; 26: 49–70.
- [36] Rong Y, Dong F, Zhang G, Tang M, Zhao X, Zhang Y, *et al.* The crosstalk of lactate-Histone lactylation and tumor. *Proteomics. Clinical Applications*. 2023; 17: e2200102.
- [37] Moreno-Yruela C, Zhang D, Wei W, Bæk M, Liu W, Gao J, *et al.* Class I histone deacetylases (HDAC1-3) are histone lysine delactylases. *Science Advances*. 2022; 8: eabi6696.
- [38] Hanahan D, Weinberg RA. Hallmarks of cancer: the next generation. *Cell*. 2011; 144: 646–674.
- [39] Lv D, Zou Y, Zeng Z, Yao H, Ding S, Bian Y, *et al.* Comprehensive metabolomic profiling of osteosarcoma based on UHPLC-HRMS. *Metabolomics: Official Journal of the Metabolomic Society*. 2020; 16: 120.
- [40] Hua Y, Qiu Y, Zhao A, Wang X, Chen T, Zhang Z, *et al.* Dynamic metabolic transformation in tumor invasion and metastasis in mice with LM-8 osteosarcoma cell transplantation. *Journal of Proteome Research*. 2011; 10: 3513–3521.
- [41] Moretton MA, Bernabeu E, Grotz E, Gonzalez L, Zubillaga M, Chiappetta DA. A glucose-targeted mixed micellar formulation outperforms Genexol in breast cancer cells. *European Journal of Pharmaceutics and Biopharmaceutics*. 2017; 114: 305–316.
- [42] Dean DC, Shen S, Hornicek FJ, Duan Z. From genomics to metabolomics: emerging metastatic biomarkers in osteosarcoma. *Cancer Metastasis Reviews*. 2018; 37: 719–731.
- [43] Ye T, Liang Y, Zhang D, Zhang X. MicroRNA-16-1-3p Represses Breast Tumor Growth and Metastasis by Inhibiting PGK1-Mediated Warburg Effect. *Frontiers in Cell and Developmental Biology*. 2020; 8: 615154.
- [44] Nema R, Shrivastava A, Kumar A. Prognostic role of lipid phosphate phosphatases in non-smoker, lung adenocarcinoma patients. *Computers in Biology and Medicine*. 2021; 129: 104141.
- [45] Perego S, Sansoni V, Banfi G, Lombardi G. Sodium butyrate has anti-proliferative, pro-differentiating, and immunomodulatory effects in osteosarcoma cells and counteracts the TNF α -induced low-grade inflammation. *International Journal of Immunopathology and Pharmacology*. 2018; 32: 394632017752240.
- [46] Holbert CE, Cullen MT, Casero RA, Jr, Stewart TM. Polyamines in cancer: integrating organismal metabolism and antitumor immunity. *Nature Reviews. Cancer*. 2022; 22: 467–480.
- [47] Rostamian H, Khakpoor-Koosheh M, Jafarzadeh L, Masoumi E, Fallah-Mehrjardi K, Tavassolifar MJ, *et al.* Restricting tumor lactic acid metabolism using dichloroacetate improves T cell functions. *BMC Cancer*. 2022; 22: 39.
- [48] Wang ZH, Peng WB, Zhang P, Yang XP, Zhou Q. Lactate in the tumor microenvironment: From immune modulation to therapy. *EBioMedicine*. 2021; 73: 103627.
- [49] Zhao YH, Zhou M, Liu H, Ding Y, Khong HT, Yu D, *et al.* Upregulation of lactate dehydrogenase A by ErbB2 through

heat shock factor 1 promotes breast cancer cell glycolysis and growth. *Oncogene*. 2009; 28: 3689–3701.

- [50] Varner EL, Trefely S, Bartee D, von Krusenstiern E, Izzo L, Bekeova C, *et al.* Quantification of lactoyl-CoA (lactyl-CoA) by liquid chromatography mass spectrometry in mammalian cells and tissues. *Open Biology*. 2020; 10: 200187.
- [51] Zhang D, Tang Z, Huang H, Zhou G, Cui C, Weng Y, *et al.* Metabolic regulation of gene expression by histone lactylation. *Nature*. 2019; 574: 575–580.
- [52] Abbaszadeh Z, Çeşmeli S, Biray Avcı Ç. Crucial players in glycolysis: Cancer progress. *Gene*. 2020; 726: 144158.
- [53] Sun S, Li H, Chen J, Qian Q. Lactic Acid: No Longer an Inert and End-Product of Glycolysis. *Physiology (Bethesda, Md.)*. 2017; 32: 453–463.
- [54] Hirschhaeuser F, Sattler UGA, Mueller-Klieser W. Lactate: a metabolic key player in cancer. *Cancer Research*. 2011; 71: 6921–6925.
- [55] Nakagawa Y, Negishi Y, Shimizu M, Takahashi M, Ichikawa M, Takahashi H. Effects of extracellular pH and hypoxia on the function and development of antigen-specific cytotoxic T lymphocytes. *Immunology Letters*. 2015; 167: 72–86.
- [56] Daverio Z, Balcerzyk A, Rautureau GJP, Panthu B. How Warburg-Associated Lactic Acidosis Rewires Cancer Cell Energy Metabolism to Resist Glucose Deprivation. *Cancers*. 2023; 15: 1417.
- [57] Li F, Simon MC. Cancer Cells Don't Live Alone: Metabolic Communication within Tumor Microenvironments. *Developmental Cell*. 2020; 54: 183–195.
- [58] Baltazar F, Afonso J, Costa M, Granja S. Lactate Beyond a Waste Metabolite: Metabolic Affairs and Signaling in Malignancy. *Frontiers in Oncology*. 2020; 10: 231.
- [59] Stošić-Grujičić S, Saksida T, Miljković Đ, Stojanović I. MIF and insulin: Lifetime companions from common genesis to common pathogenesis. *Cytokine*. 2020; 125: 154792.
- [60] Cheng B, Wang Q, Song Y, Liu Y, Liu Y, Yang S, *et al.* MIF inhibitor, ISO-1, attenuates human pancreatic cancer cell proliferation, migration and invasion in vitro, and suppresses xenograft tumour growth in vivo. *Scientific Reports*. 2020; 10: 6741.
- [61] He XX, Yang J, Ding YW, Liu W, Shen QY, Xia HHX. Increased epithelial and serum expression of macrophage migration inhibitory factor (MIF) in gastric cancer: potential role of MIF in gastric carcinogenesis. *Gut*. 2006; 55: 797–802.
- [62] Verjans E, Noetzel E, Bektas N, Schütz AK, Lue H, Lennartz B, *et al.* Dual role of macrophage migration inhibitory factor (MIF) in human breast cancer. *BMC Cancer*. 2009; 9: 230.
- [63] Mawhinney L, Armstrong ME, O' Reilly C, Bucala R, Leng L, Fingerle-Rowson G, *et al.* Macrophage migration inhibitory factor (MIF) enzymatic activity and lung cancer. *Molecular Medicine (Cambridge, Mass.)*. 2015; 20: 729–735.
- [64] Zhang H, Ye YL, Li MX, Ye SB, Huang WR, Cai TT, *et al.* CXCL2/MIF-CXCR2 signaling promotes the recruitment of myeloid-derived suppressor cells and is correlated with prognosis in bladder cancer. *Oncogene*. 2017; 36: 2095–2104.
- [65] Ye L, Jiang Y, Zhang M. Crosstalk between glucose metabolism, lactate production and immune response modulation. *Cytokine & Growth Factor Reviews*. 2022; 68: 81–92.
- [66] Ding Y, Liu Z, Desai S, Zhao Y, Liu H, Pannell LK, *et al.* Receptor tyrosine kinase ErbB2 translocates into mitochondria and regulates cellular metabolism. *Nature Communications*. 2012; 3: 1271.
- [67] Liu Y, Huang Y, Zhang J, Pei C, Hu J, Lyu J, *et al.* TIMMDC1 Knockdown Inhibits Growth and Metastasis of Gastric Cancer Cells through Metabolic Inhibition and AKT/GSK3 β /Catenin Signaling Pathway. *International Journal of Biological Sciences*. 2018; 14: 1256–1267.
- [68] Kaminski M, Kiessling M, Süß D, Krammer PH, Gülow K. Novel role for mitochondria: protein kinase C θ -dependent oxidative signaling organelles in activation-induced T-cell death. *Molecular and Cellular Biology*. 2007; 27: 3625–3639.
- [69] Trotta AP, Chipuk JE. Mitochondrial dynamics as regulators of cancer biology. *Cellular and Molecular Life Sciences: CMLS*. 2017; 74: 1999–2017.
- [70] Kelleher FC, O'Sullivan H. Monocytes, Macrophages, and Osteoclasts in Osteosarcoma. *Journal of Adolescent and Young Adult Oncology*. 2017; 6: 396–405.
- [71] Vaupel P, Multhoff G. Revisiting the Warburg effect: historical dogma versus current understanding. *The Journal of Physiology*. 2021; 599: 1745–1757.
- [72] Cho O, Lee JW, Kim HS, Jeong YJ, Heo TH. Chelerythrine, a novel small molecule targeting IL-2, inhibits melanoma progression by blocking the interaction between IL-2 and its receptor. *Life Sciences*. 2023; 320: 121559.
- [73] Seneviratne JA, Carter DR, Mitra R, Gifford A, Kim PY, Luo JS, *et al.* Inhibition of mitochondrial translocase SLC25A5 and histone deacetylation is an effective combination therapy in neuroblastoma. *International Journal of Cancer*. 2023; 152: 1399–1413.